Soliton trapping in a disordered lattice

Zhi-Yuan Sun* and Shmuel Fishman†
Department of Physics, Technion–Israel Institute of Technology, Haifa 32000, Israel

Avy Soffer‡
Department of Mathematics, Rutgers University, Piscataway, New Jersey 08854, USA
(Received 18 January 2015; revised manuscript received 11 May 2015; published 1 July 2015)

In recent years, the competition between randomness and nonlinearity was extensively explored. In the present paper, the dynamics of solitons of the Ablowitz-Ladik model in the presence of a random potential is studied. In the absence of the random potential, it is an integrable model and the solitons are stable. As a result of the random potential, this stability is destroyed. In a certain regime, for short times, particlelike dynamics with constant mass is found; in another regime, particlelike dynamics with varying mass takes place. In particular, an effective potential is found that predicts correctly changes in the direction of motion of the soliton. This potential is a scaling function of time and strength of the potential, leading to a relation between the first time when the soliton changes direction and the strength of the random potential.

DOI: 10.1103/PhysRevE.92.012901 PACS number(s): 05.45.Yv, 42.65.Tg

I. INTRODUCTION

Solitons are one of the most remarkable manifestations of nonlinearity. They are found for continuous systems for the nonlinear Schrödinger equation (NLSE) in one dimension [1]. On the lattice, mobile solitons are found for the model introduced by Ablowitz and Ladik (AL) [2], while for the ordinary NLSE on a lattice, a mobile soliton is only an approximate concept. Disorder tends to affect and typically destroy solitons both on a lattice and in the continuum. In the present work, this will be studied for a one-dimensional (1D) lattice in the framework of the AL model.

For the continuous system, early numerical work of Bronski [3] indicates that a NLSE soliton becomes trapped in the random media when its kinetic energy decreases sufficiently and is of comparable size to the background potential. Akkermans *et al.* [4] show numerically that a soliton bounces back and forth between high potential barriers in attractive Bose-Einstein condensates in the framework of the Gross-Pitaevskii equation with strong disorder. In addition, like the Anderson localization of linear waves in random media, some authors relate the localization of solitons in a disordered environment to *Anderson localization* [5,6].

In the absence of a random potential, the AL model is

$$i\frac{\partial \psi_n}{\partial t} = -(\psi_{n-1} + \psi_{n+1})(1 + |\psi_n|^2), \tag{1}$$

where ψ_n is the wave function on site n at time t. The AL model is an integrable discrete version of the continuous NLSE, while the discrete version of the ordinary NLSE is nonintegrable. This relates the AL model to many physical systems, for instance in the nonlinear waveguide arrays [7,8] and discrete molecular chains [9,10]. The integrability of the AL model is manifested by the existence of a mobile soliton solution [11,12],

$$\psi_n(t) = \frac{\sinh(\mu)}{\cosh[\mu(n-x)]}\exp[ik(n-x) + i\alpha], \tag{2}$$

where the time-dependent parameters x and α can be expressed as

$$\dot{x} = 2\frac{\sinh(\mu)}{\mu}\sin(k), \tag{3a}$$

$$\dot{\alpha} = 2\left[\cosh(\mu)\cos(k) + \frac{k}{\mu}\sinh(\mu)\sin(k)\right]. \tag{3b}$$

From (2) we see that $\frac{1}{\mu}$ characterizes the width of the soliton and x is its center. On the other hand, the AL equation has two conserved quantities, the first of which can be defined as the mass of the soliton solution [11–13],

$$M_s = \sum_{n=-\infty}^{\infty} \ln(1 + |\psi_n|^2), \tag{4}$$

while the second can be defined as the momentum of the motion [11–13],

$$P = i\sum_{n=-\infty}^{\infty}(\psi_n\psi_{n+1}^* - \psi_n^*\psi_{n+1}), \tag{5}$$

where $*$ denotes the complex conjugation. For the soliton solution (2), we can calculate that (see also the Appendix of [11])

$$M_s = 2\mu \tag{6}$$

and

$$P = M_s\dot{x} = 4\sinh(\mu)\sin(k). \tag{7}$$

Therefore, M_s can indeed be considered as the mass of the soliton.

In the present work, we will study solitons for the AL model with a random potential defined by

$$i\frac{\partial \psi_n}{\partial t} = -(\psi_{n-1} + \psi_{n+1})(1 + |\psi_n|^2) + \varepsilon_n\psi_n, \tag{8}$$

*sunzhiyuan137@aliyun.com
†fishman@physics.technion.ac.il
‡soffer@math.rutgers.edu

where ε_n are independent random variables uniformly distributed in the interval $[-\frac{W}{2}, \frac{W}{2}]$. This is the disordered version of (1). The disordered NLSE,

$$i\frac{\partial \psi_n}{\partial t} = -(\psi_{n-1} + \psi_{n+1}) + \varepsilon_n \psi_n + \beta|\psi_n|^2\psi_n, \qquad (9)$$

is a paradigm for the exploration of the competition between the effects of disorder that are tending to localize, and those of nonlinearity that are tending to enhance spreading (for a review, see [14]). Most of the work on (9) addressed this conceptional problem. It was motivated by the exploration of transport in optical waveguides, where a component of the electric field plays the role of the wave function [8], and by the dynamics of cold atoms in disordered potentials [15]. The hope is that many qualitative results obtained in the framework of (8) will hold also for (9). In the exploration of (8), we can take advantage of the fact that in the absence of disorder, (8) reduces to (1), which is integrable.

For the continuous version, two early reviews [16,17] have addressed the propagation of solitons in disordered systems; in the works by Bronski [3,18] and Garnier [19], they show two regimes for the NLSE soliton propagation. In one regime, the soliton mass decays while its velocity approaches a constant; in the other regime, the soliton mass approaches a constant while its velocity decays very slowly. Garnier further applied a perturbation theory of the inverse scattering transform to confirm that two similar regimes are found for the AL solitons with on-site random potential (in the limit of zero randomness) [20]. Which regime is relevant depends on the value of the initial mass of the AL soliton. For large μ, the mass approaches a constant, while for small μ, the velocity approaches a constant.

However, we will show numerically, for the weak randomness, that the large soliton will be trapped before its velocity decreases to zero. Additionally, we will find a regime in which the AL soliton has the possibility to be accelerated on average by the specific randomness. We will also characterize the regime in which the soliton can be trapped by the disorder using a particle approach, i.e., where the soliton can be considered as a particle.

The outline of the paper is as follows. In Sec. II, the dynamics is classified by the initial value of the soliton mass. In Sec. III, a regime where the soliton can be considered as a particle is studied; in Sec. IV, a scaling dependence of the time when the soliton is trapped is found to scale with the strength of the random potential W. The results are summarized in Sec. V.

II. SOLITON PROPAGATION IN A DISORDERED LATTICE

In this section, we will study the solution of Eq. (8) numerically and semianalytically in order to develop an intuitive picture of the soliton dynamics. The initial soliton is the one found for a chain without disorder, given by (2), with

$$x = 0, \ \dot{x} > 0, \qquad (10a)$$

$$M_s(t=0) = 2\mu_0, \qquad (10b)$$

$$\mu_0 = \mu(t=0). \qquad (10c)$$

The numerical solution is obtained propagating the soliton by Eq. (8). To save computer resources, we use a coordinate system moving with the center of mass of the soliton, consisting of N sites centered on the soliton. The computation is performed using a fourth-order Runge-Kutta-type algorithm in time and an absorbing-wave boundary condition. In Appendix C, the validity of the method for the parameters used is verified. We define the following quantities:

Soliton mass,

$$M_s^{(N)} = \sum_n^N \ln(1 + |\psi_n|^2), \qquad (11)$$

center-of-mass coordinate,

$$x^{(N)} = \sum_n^N n \ln(1 + |\psi_n|^2)/M_s^{(N)}, \qquad (12)$$

and the second moment,

$$m_2^{(N)} = \sum_n^N (n - x^{(N)})^2 \ln(1 + |\psi_n|^2), \qquad (13)$$

while the soliton velocity is

$$v = \Delta x^{(N)}/\Delta t, \qquad (14)$$

where $\Delta x^{(N)}$ is the change of $x^{(N)}$ during the time interval Δt (here we use $\Delta t = 0.001$). In addition, two parameters that characterize the soliton are introduced in the simulation: one is the amplitude of the soliton,

$$A_s = \max_n |\psi_n|^2, \qquad (15)$$

while the other is the soliton width, defined as the minimum N_w satisfying

$$\sum_{-(N_w-1)/2}^{(N_w-1)/2} \ln(1 + |\psi_n|^2)/M_s^{(N)} \geqslant 1 - \delta, \qquad (16)$$

where $\delta = 0.01$ [note that in the simulation, we first find the peak position of the soliton, and then (16) is calculated with this position as the center].

There are basically three regimes characterized by the initial value of μ:

$$\text{(A)} \ \mu_0 \gg 1, \qquad (17a)$$

$$\text{(B)} \ \mu_0 \approx 1, \qquad (17b)$$

$$\text{(C)} \ \mu_0 \ll 1. \qquad (17c)$$

A. The regime $\mu_0 \gg 1$

We choose an AL soliton with $\mu_0 = 3$, which has more than 99% mass concentrating in three lattice sites ($N_w = 3$). The reason for picking up a soliton of such narrow width is based on the fact that it is compact enough to admit a low level of mass radiation due to randomness. Such low-level radiation is necessary for observing possible soliton acceleration in our numerical simulation. The initial velocity of the soliton is chosen as $\dot{x}(t=0) = 1$, and one specific realization of the random potential with $W = 0.1$ is used. Note

that $0.04 \lesssim W \lesssim 0.1$ can be seen as the weak randomness in our discussion. However, if randomness is very weak, the soliton dynamics may not be distinguished from that in the limit of zero randomness as in [20].

Assuming the random potential is a perturbation, the approximate equations for the various parameters in this potential can be derived following the work of Cai *et al.* [11]. The resulting equations derived in Appendix A are

$$\dot{\mu} = 0, \tag{18a}$$

$$\dot{x} = \frac{2\sinh(\mu)}{\mu}\sin(k), \tag{18b}$$

$$\dot{k} = -\sinh^2(\mu)\sum_{n=-\infty}^{+\infty}\frac{\varepsilon_n \tanh[\mu(n-x)]}{\cosh[\mu(n+1-x)]\cosh[\mu(n-1-x)]}, \tag{18c}$$

$$\dot{\alpha} = 2\left[\cosh(\mu)\cos(k) + \frac{k}{\mu}\sinh(\mu)\sin(k)\right] + \sinh^2(\mu)\sum_{n=-\infty}^{+\infty}\frac{\varepsilon_n(n-x)\tanh[\mu(n-x)]}{\cosh[\mu(n+1-x)]\cosh[\mu(n-1-x)]} - \sinh(\mu)\cosh(\mu)\sum_{n=-\infty}^{+\infty}\frac{\varepsilon_n}{\cosh[\mu(n+1-x)]\cosh[\mu(n-1-x)]}. \tag{18d}$$

Equations (18) are integrated numerically with the initial conditions (10). The algorithm used is the fourth-order Runge-Kutta with $\Delta t = 0.001$, and the summations are truncated to a finite window around the center of mass of the soliton. The values of the parameters μ, k, x, and α are inserted in (2). We refer to this solution as the semianalytical solution. We compare this solution with the numerical integration of Eq. (8) (referred to as the numerical solution), and the results are presented in Fig. 1. In Fig. 1(a), we compare the center-of-mass coordinate x of (2) and (12) found in the semianalytical calculation with the numerical solution. It is found that on average, the velocity of the semianalytical solution is somewhat larger than that found numerically. In Fig. 1(b), the velocity of the center of mass and the second moment are presented. The plots for the velocity are zoomed in Figs. 1(c)–1(e), and the soliton profiles are shown in Fig. 1(f). We note that for $t < 100$ there is excellent agreement between the numerical and the semianalytical results. At time $t > 100$, the second moment increases rapidly, therefore the approximation (18) is not justified anymore, and a large deviation between the two solutions is shown.

B. The regime $\mu_0 \approx 1$

As a representative example in this regime, we study a soliton with $\mu_0 = 1$, moving in one realization of the random potential with $W = 0.1$. We solve numerically Eq. (8) with the initial condition (10). In this case, the initial width of the soliton is seven sites ($N_w = 7$). The results are presented in Fig. 2. We find that the center of mass x moves monotonically to the right until time $t = T_c$, when oscillations start [see Fig. 2(a)]. From Fig. 2(b), we see that the velocity decreases monotonically for $t < T_c$ and oscillates for $t > T_c$. The period of these oscillations decreases with time. From Fig. 2(c) we see that the mass decreases with time and in the first stage this decrease is rapid, therefore the approximation (18) fails. Finally, the mass approaches a nonvanishing constant. Figure 2(d) presents the soliton profiles. The interesting phenomenon we find is the trapping of the soliton for $t > T_c$ as a result of randomness. Such trapping is a general soliton behavior, and it is not specific to any realization of randomness, as we tested explicitly. In Fig. 2(e), we show the averaged soliton velocity $v^{(\mathrm{av})}$ and mass $M_s^{(\mathrm{av})}$ over 12 realizations of the random potential. The general features are similar to those found for specific realizations, but the oscillations in Fig. 2(b) are washed out by the averaging. The particle aspect of this dynamics in this regime will be discussed in the next section.

C. The regime $\mu_0 \ll 1$

In this regime, the soliton has a larger width, and it is easier to lose its mass through radiation. With a limit of zero randomness, Garnier [20] shows that the soliton propagates with its mass decreasing to zero and its velocity decreasing to a nonvanishing constant. In fact, the radiation induces a remarkable deformation on the soliton profile after some time of propagation if the randomness is not weak enough. In Fig. 3, we present an example with $\mu_0 = 0.5$ [where the initial width of the soliton is 11 sites ($N_w = 11$)] and $W = 0.1$. The initial condition is (10). From Fig. 3(a) we see that the soliton spreads and radiates its mass over 300 sites in the time $t = 1000$. From Figs. 3(b) and 3(c) we conclude that the mass and velocity decrease. Such a decrease of velocity includes some short time intervals where the velocity oscillates approximately near a constant. Similar time intervals have been observed in the work of Franzosi *et al.* [21], as they studied the mobile discrete breathers propagating on very weak backgrounds in the framework of a discrete NLSE. Their time intervals appear to be much longer, with weaker velocity oscillations, since their background perturbation is very weak. Similar qualitative behavior was found for different realizations of the random potential. Moreover, Fig. 3(d) shows the averaged soliton velocity and mass over 12 realizations of random potentials. We have not observed the trapping behavior in this regime, especially before the soliton undergoes a large deformation.

III. PARTICLE APPROACH FOR SOLITON TRAPPING IN A DISORDERED AL LATTICE

In this section, we will study the following question: Can an AL soliton in a weak random potential be considered as particle?

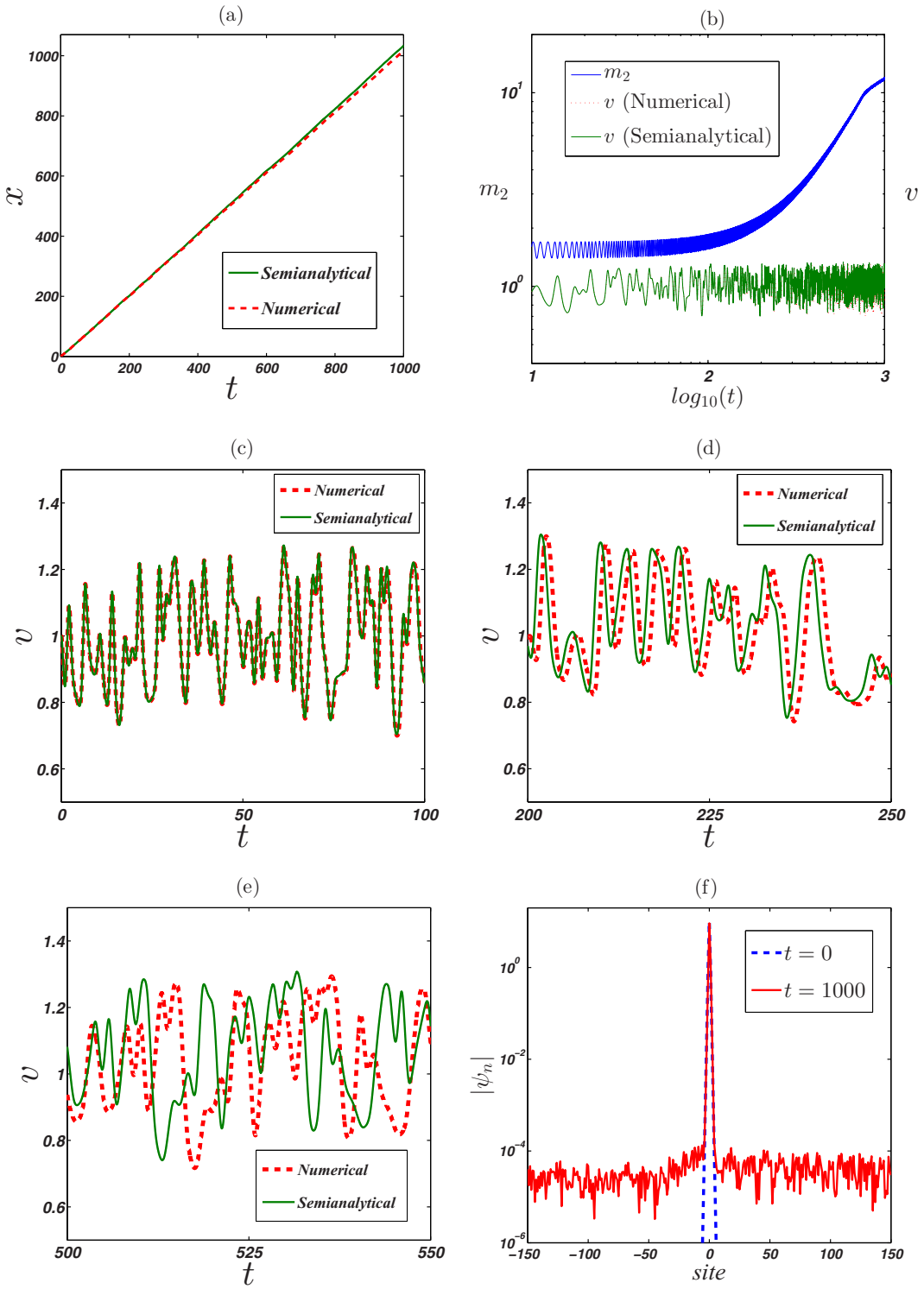

FIG. 1. (Color online) AL soliton acceleration by one specific realization of the random potential [$\mu_0 = 3$, $v(t = 0) = 1$, and $W = 0.1$]. (a) Comparison of the center of mass between the semianalytical (solid green line) and numerical (dashed red line) results. (b) Comparison of the semianalytical (lower solid green line) and numerical (lower dashed red line) velocities, and the second moment m_2 (upper solid blue line). (c)–(e) Zoomed views of the velocity comparison in three different time intervals. (f) The soliton profiles at $t = 0$ (dashed blue line) and $t = 1000$ (solid red line). Note that the site coordinate is fixed on the center of mass.

We will focus on the soliton trapping in the second regime where $\mu_0 \approx 1$, and we will try to give a particle description of the trapping behavior. We start from the momentum (5), and we assume it is still the momentum for the model (8) when the random potential is weak. Taking a derivative on both sides of Eq. (5) with respect to t, and substituting Eq. (8) into the

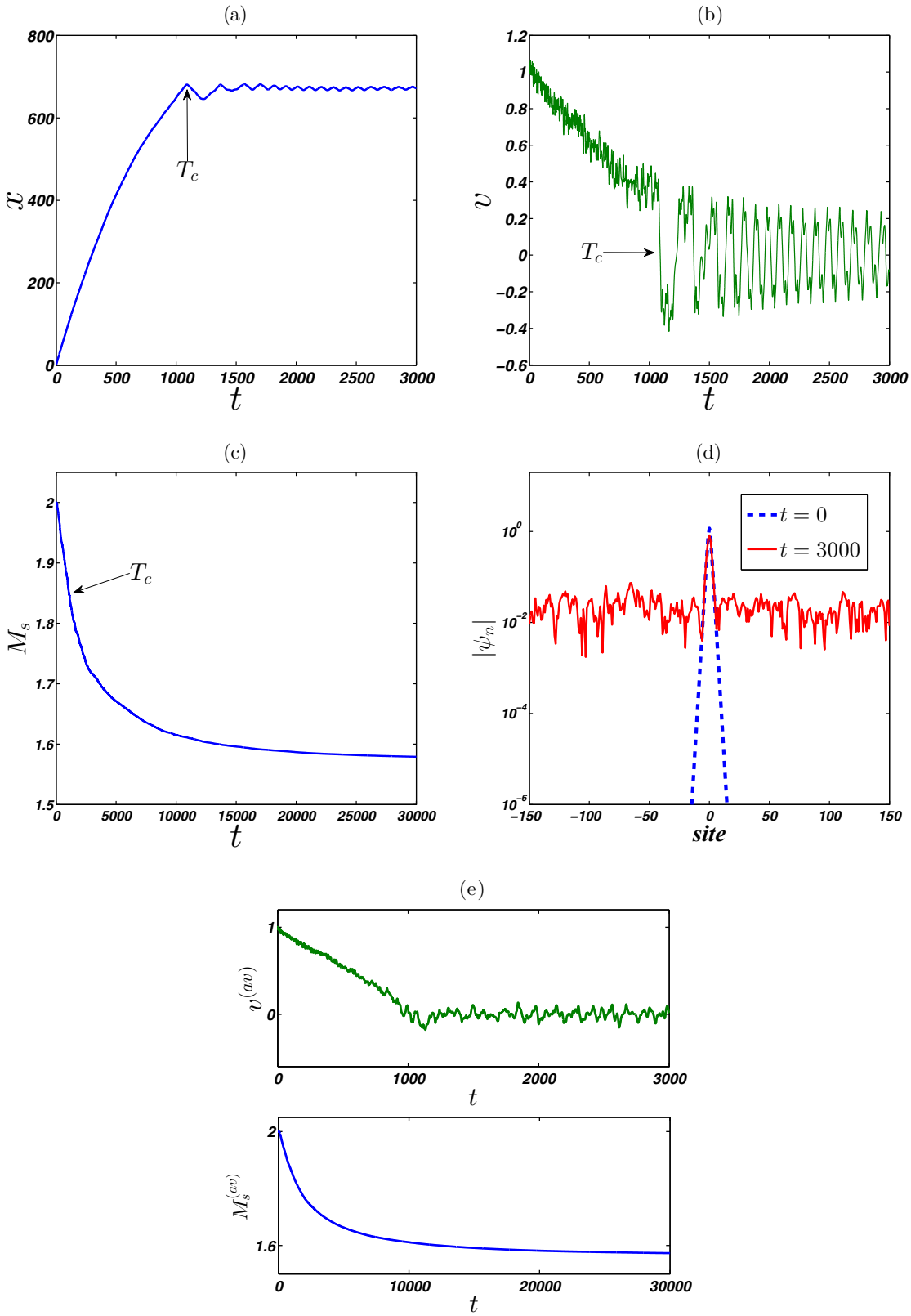

FIG. 2. (Color online) AL soliton trapping by one realization of the random potential [$\mu_0 = 1$, $v(t = 0) = 1$, and $W = 0.1$]. (a) Center of mass x [Eq. (12)] as a function of time t. (b) The soliton velocity v [Eq. (14)] as a function of time t. (c) The mass M_s [Eq. (11)] as a function of time t. (d) The soliton profiles at $t = 0$ (dashed blue line) and $t = 3000$ (solid red line). (e) $v^{(\mathrm{av})}$ and $M_s^{(\mathrm{av})}$ as a function of time t (the averaging is performed over 12 realizations).

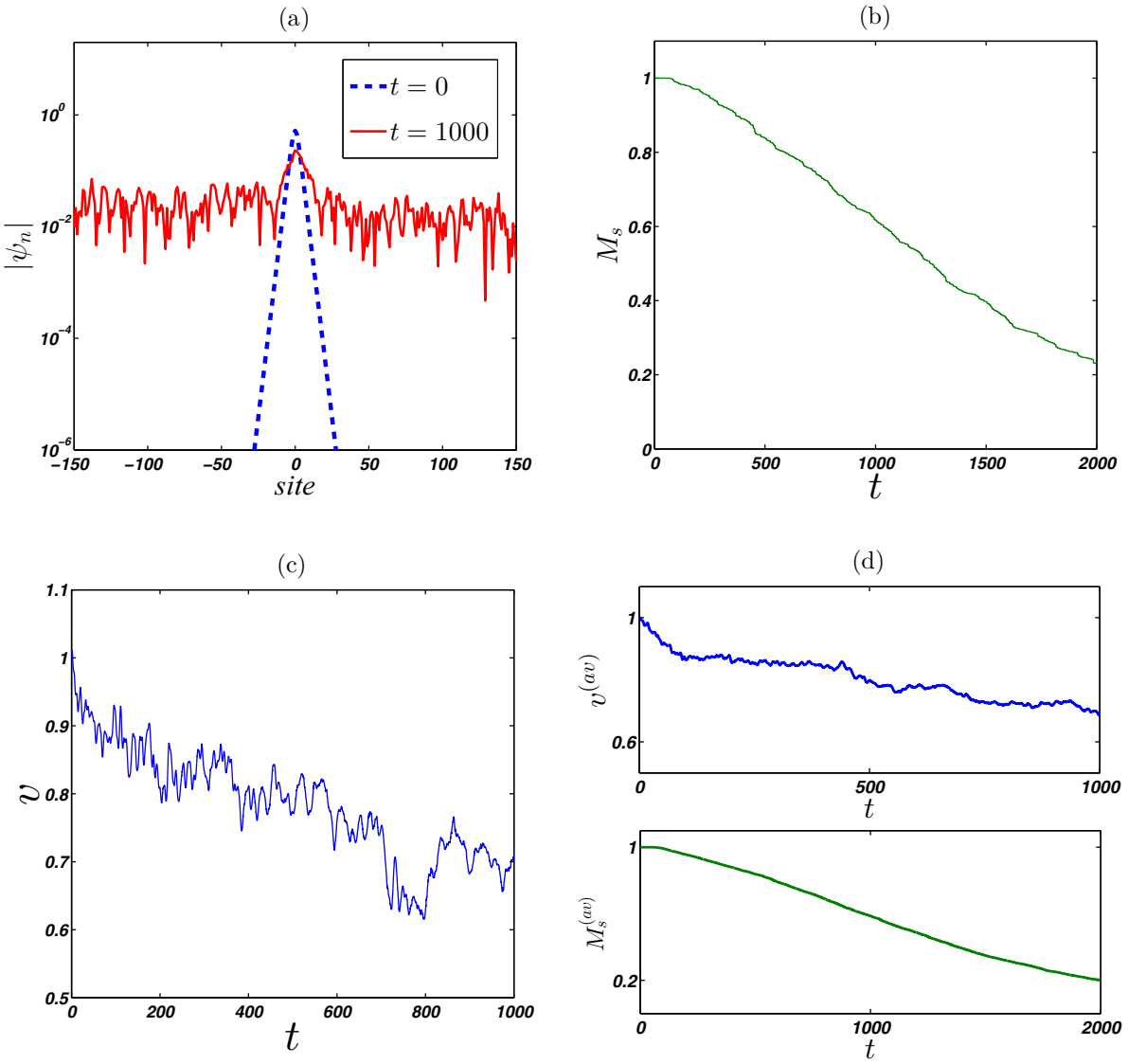

FIG. 3. (Color online) AL soliton propagation in one realization of the random potential [$\mu_0 = 0.5$, $v(t = 0) = 1$, and $W = 0.1$]. (a) The soliton profiles at $t = 0$ (dashed blue line) and $t = 1000$ (solid red line). (b) The mass M_s [Eq. (11)] as a function of time t. (c) The soliton velocity v [Eq. (14)] as a function of time t. (d) $v^{(\mathrm{av})}$ and $M_s^{(\mathrm{av})}$ as a function of time t (the averaging is performed over 12 realizations).

result, we can obtain

$$\frac{dP}{dt} = 2\sum_{n=-\infty}^{+\infty} \mathrm{Re}(\psi_n \psi_{n+1}^*)(\varepsilon_n - \varepsilon_{n+1}), \tag{19}$$

where Re means the real part. For derivation, see Appendix B. With the assumption that the soliton is particlelike, Eq. (19) can be viewed as the variation rate of its momentum. On the other hand, dP/dt from (7) can also be written as

$$\frac{dP}{dt} = \frac{dM_s}{dt}v + M_s\frac{d^2x}{dt^2}. \tag{20}$$

Notice that, due to the mass radiation, the term dM_s/dt in Eq. (20) cannot be neglected, especially before soliton trapping. Therefore, we can write the randomness-generated *force* in two ways. One is directly

$$F_1 = M_s\frac{d^2x}{dt^2}, \tag{21}$$

and the other one can be derived using (19) and (20)

$$F_2 = 2\sum_{n=-\infty}^{+\infty} \mathrm{Re}(\psi_n \psi_{n+1}^*)(\varepsilon_n - \varepsilon_{n+1}) - \frac{dM_s}{dt}v. \tag{22}$$

The test of the particlelike picture is performed by comparing the forces F_1 and F_2 presented in Fig. 4. Excellent agreement is found. These results strongly support the description of solitons as particles. In this picture with the force F_2 we associate work done on the soliton that decreases its kinetic energy with an effective potential,

$$U(t) = U_0 - \int_{t_0}^{t} F_2 v\, dt', \tag{23}$$

where U_0 is a parameter that can be viewed as the initial energy to be determined as the constant that leads the mean of U, over the time interval of trapping in simulations, to be zero, i.e., $U_0 = \langle \int_{t>T_c} F_2 v\, dt \rangle$. With the same data, we plot both of this effective potential $U(t)$ and soliton velocity in

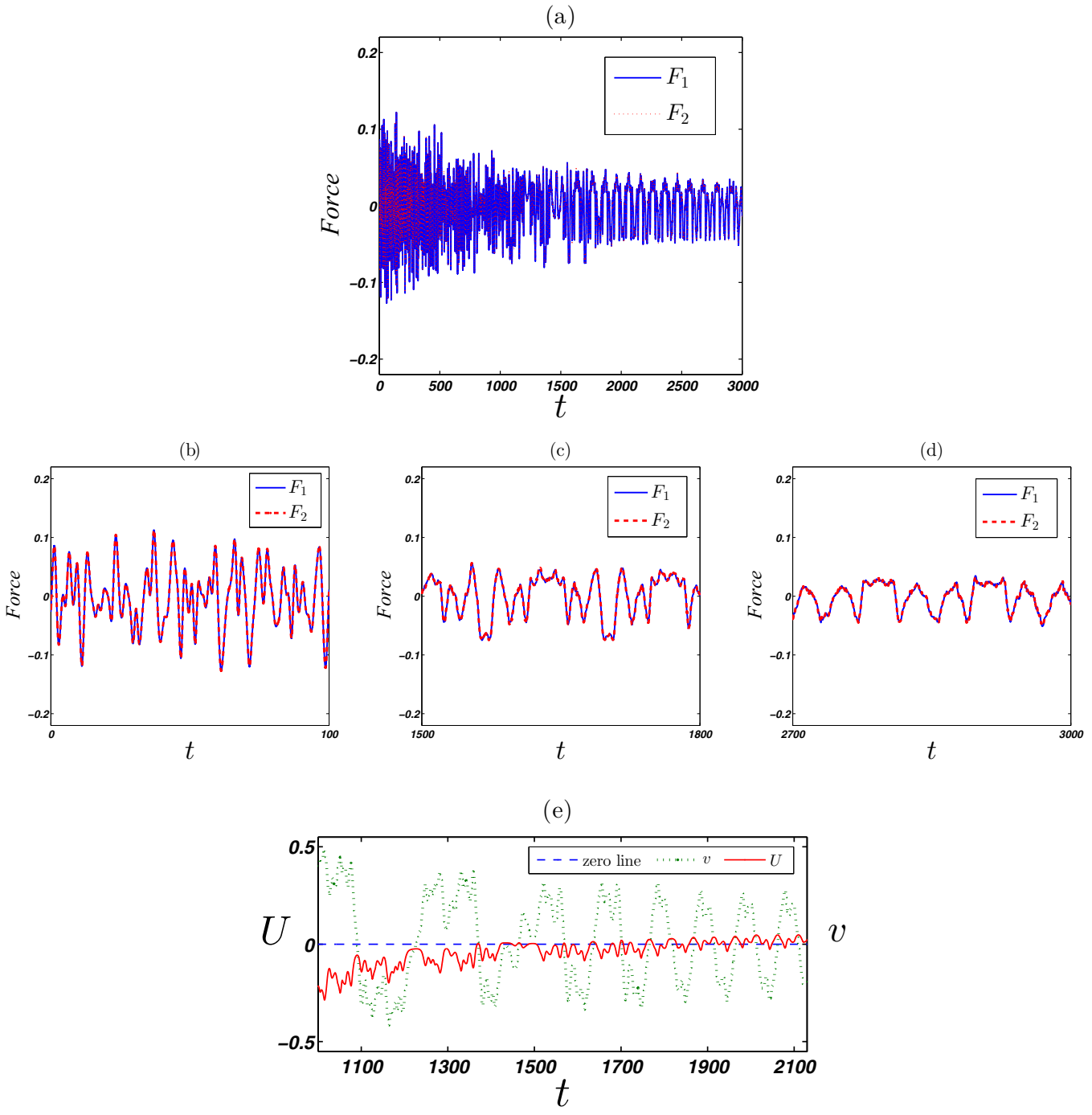

FIG. 4. (Color online) (a) Comparison of the two forces F_1 [Eq. (21)] (solid blue line) and F_2 [Eq. (22)] (dashed red line) with the soliton parameters and random potential the same as those in Figs. 2(a) and 2(b). (b)–(d) Zoomed views of panel (a) for three different time intervals. (e) The effective potential U (solid red line) and soliton velocity v (dotted green line) after the soliton's first reflection ($T_c \approx 1100$).

Fig. 4(e). It shows that the first reflection ($T_c \approx 1100$), with the soliton velocity changing its sign, occurs at a peak position of the effective potential. Also other changes in the direction of motion of the soliton take place at maxima of $U(t)$, as can be seen from Fig. 4(e). This is a direct result of (23) since

$$\frac{dU(t)}{dt} = -vF_2, \tag{24}$$

therefore $\frac{dU(t)}{dt} = 0$ implies either $F_2 = 0$ or $v = 0$.

We note that for $t > T_c$, the soliton is trapped and oscillates in space. This is localization that can be described completely classically, as it results from a potential. Therefore, it differs from the Anderson localization of solitons claimed in earlier works [6,22,23]. Sacha *et al.* [6,23] studied a quasi-one-dimensional bright matter-wave soliton in a spatially correlated disordered potential. They find that the soliton shape is hardly affected when the potential is weak and smooth, but the quantum motion of the soliton's center of mass displays Anderson localization. A similar investigation on dark solitons

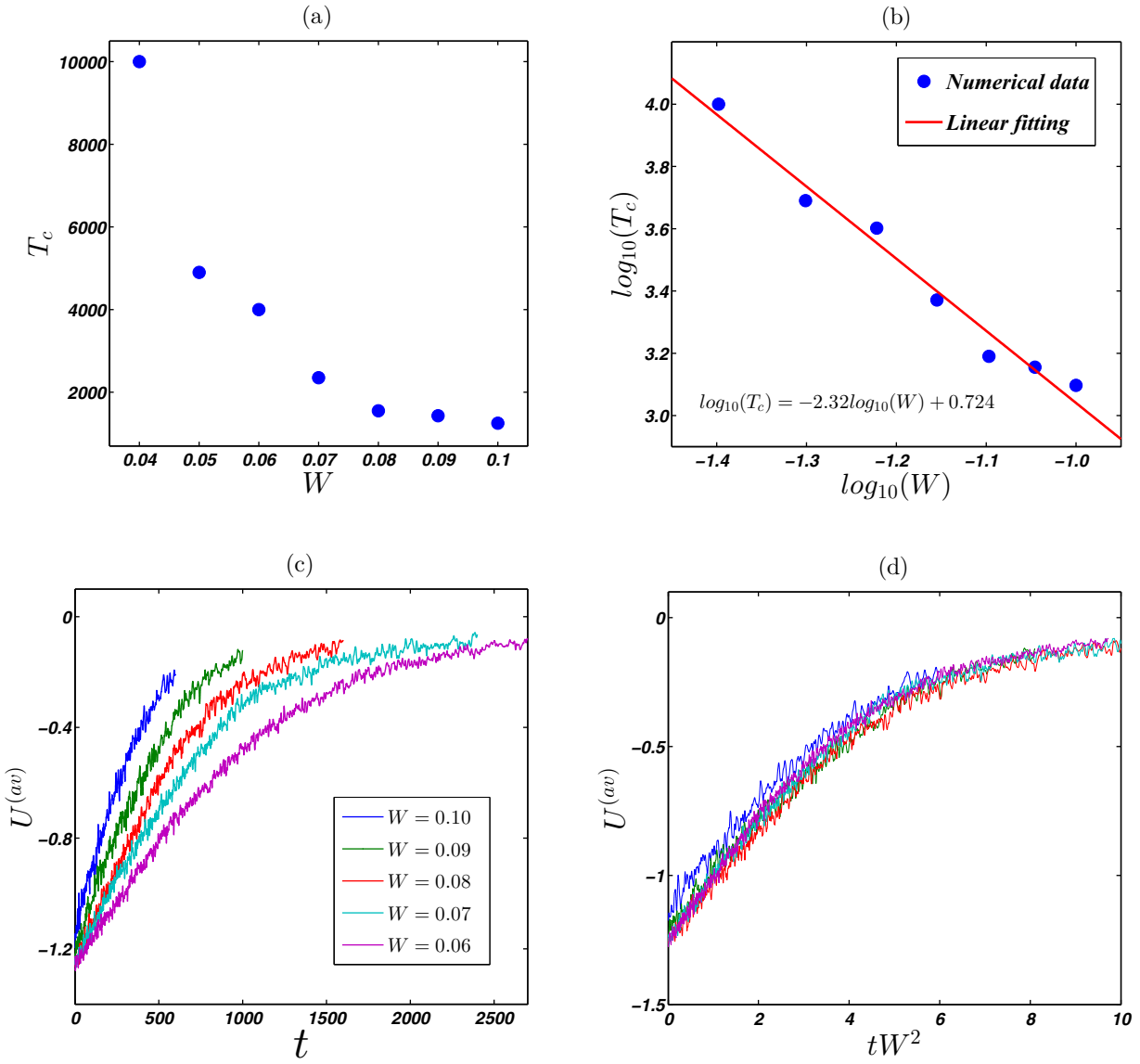

FIG. 5. (Color online) (a) T_c as function of W. The random potentials are constructed of one realization of random numbers in $[-1,1]$, multiplied by different strength $W/2$. (b) Linear fit of the data (logarithm forms of variables) in (a). (c) $U^{(\mathrm{av})}$ as a function of t and W (the lines from left to right correspond to W from 0.10 to 0.06). (d) $U^{(\mathrm{av})}$ as a function of the scaling variable tW^2.

was performed by Mochol *et al.* [22]. Our case is completely classical. It consists of two stages: one is for $t < T_c$, where the soliton propagates losing its mass and kinetic energy, however the kinetic energy is still much larger than the random potential (as we checked explicitly); the other one is for $t > T_c$, where the soliton is trapped and localized by the randomness, with its kinetic energy comparable to the random potential. Both stages can be described using a particle with varying mass moving in an effective random potential, as shown in Sec. III.

IV. SCALING OF THE TRAPPING TIME T_c

In this section, we demonstrate that there exists a scaling relation between the time T_c when the trapping starts and the random potential strength W. In Figs. 5(a) and 5(b), T_c is plotted as a function of W. It is found that

$$T_c \sim W^{-\eta}, \tag{25}$$

with $\eta = 2.32 \pm 0.41$. For each $W \in [0.06, 0.1]$, we average the function $U(t)$ of (23) over six different realizations to derive $U^{(\mathrm{av})}(t)$, and we plot it up to the minimum value of T_c of six realizations in Fig. 5(c). From Fig. 5(d), we see that $U^{(\mathrm{av})}$ is related to W and t via the combination tW^2. This suggests the scaling relation

$$U^{(\mathrm{av})} \approx \Gamma(tW^2), \tag{26}$$

where Γ is the scaling function. If trapping starts at the same value of Γ, one finds

$$T_c \propto W^{-2}. \tag{27}$$

Here we want to make some comments on T_c. In the calculation of (25), we use one realization of random numbers

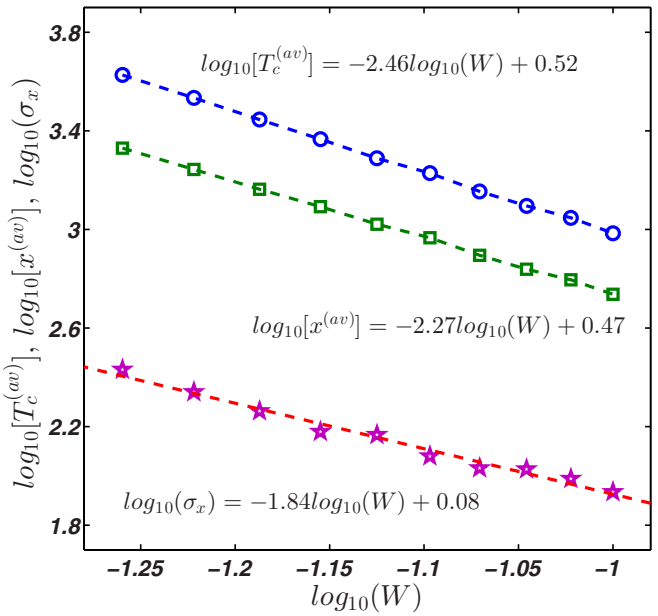

FIG. 6. (Color online) $T_c^{(\mathrm{av})}$ (blue circles), $x^{(\mathrm{av})}$ (green squares), and σ_x (red stars) as functions of W (linear fit of the logarithm of variables). The averaging is carried out over 250 realizations of the random potential. The initial soliton parameters are $\mu_0 = 1$ and $v(t=0) = 1$.

uniformly distributed in $[-1,1]$, but multiplied by the strength $W/2$, as the random potential. Since the change of T_c is obvious for small variations of W [see Figs. 5(a) and 5(b)], it can generally reflect the scaling relation. In the following, we will use multiple realizations of random potentials, in the statistical sense, to briefly study the trapping of solitons in the regime $t > T_c$.

The time T_c can be viewed as a time when the soliton enters the trapping regime, and it should relate to the classical localization. We define the following quantity $\widetilde{x}$ for any realization of the random potential:

$$\widetilde{x} = \frac{1}{T_\infty - T_c} \int_{T_c}^{T_\infty} x(t)dt, \tag{28}$$

where T_∞ is the upper boundary of time in numerical simulation. Therefore, for each W, we can derive the statistical averaging $T_c^{(\mathrm{av})} = \langle T_c \rangle$ and $x^{(\mathrm{av})} = \langle \widetilde{x} \rangle$, as well as its standard derivation $\sigma_x = [\langle (\widetilde{x} - x^{(\mathrm{av})})^2 \rangle]^{1/2}$, where $\langle \cdot \rangle$ is the averaging over realizations of the random potential. These averaged parameters provide information about the localization of solitons. We carried out the average over 250 realizations of random potentials for each W, with the results shown in Fig. 6, and we found that these parameters scale with W as

$$T_c^{(\mathrm{av})} \sim W^{-\eta_1}, \quad \eta_1 = 2.46 \pm 0.04, \tag{29a}$$
$$x^{(\mathrm{av})} \sim W^{-\eta_2}, \quad \eta_2 = 2.27 \pm 0.04, \tag{29b}$$
$$\sigma_x \sim W^{-\eta_3}, \quad \eta_3 = 1.84 \pm 0.20, \tag{29c}$$

$T_\infty = 10^4$ was used.

From the scaling coefficients, one may conclude that T_c is closely related to $\widetilde{x}$ rather than to σ_x. This is reasonable, since in fact the trapping time T_c is when the soliton's kinetic energy decreases to the same magnitude as the random potential energy (as we checked explicitly). The standard derivation, on the other hand, reflects the variation of position for $t > T_c$.

For very weak disorder, $W \lesssim 0.04$, the scaling (27) seems not to be valid. The soliton seems to lose its velocity while keeping its mass nearly constant. In particular, $T_c \approx 10^5$ for $W = 0.02$.

V. SUMMARY AND CONCLUSIONS

The dynamics of solitons in random potentials was studied in the framework of the Ablowitz-Ladik model [2]. In particular, we explored the question of when a soliton can be considered as a particle, and what the conditions are for the trapping of solitons in a random potential. The behavior was classified into three regimes specified by Eq. (17). In the regime $\mu_0 \gg 1$ for short times, approximation (18) holds. In particular, μ changes in time, resulting in the change of the soliton width. This destroys the semianalytic solution resulting from (18), as is clear from Fig. 1. For $\mu_0 \ll 1$, the soliton spreads very quickly and the potential picture is not appropriate.

The most interesting regime is when $\mu_0 \approx 1$, where the soliton is trapped and moves as a particle with varying mass. The equality of $F_1 = F_2$ that is demonstrated in Fig. 4 is strong evidence for the particle nature. The velocity changes its direction at some maxima of the potential (23), as can be seen from Fig. 4(e) and as expected from (24). A better understanding of the potential $U(t)$ and its relation to the average of the random potential over the profile of the soliton will be left for future studies. Finally, we found that T_c scales with the strength of the random potential according to (26), and the potential is a scaling function of the time and strength of the random potential.

ACKNOWLEDGMENTS

The comments from the referees are greatly appreciated. Z.-Y.S. acknowledges the partial support at Technion under a fellowship of the Israel Council for Higher Education. This work was partly supported by the Israel Science Foundation (ISF-1028), by the U.S.-Israel Binational Science Foundation (BSF-2010132), by the U.S. National Science Foundation (NSF DMS 1201394), and by the Shlomo Kaplansky academic chair.

APPENDIX A

Reference [11] shows that for an AL model with a perturbation term,

$$i\frac{\partial \psi_n}{\partial t} = -(\psi_{n-1} + \psi_{n+1})(1 + |\psi_n|^2) + R_n, \tag{A1}$$

the soliton parameters in (2) in the adiabatic approximation satisfy the following evolution equations:

$$\dot{\mu} = \sinh(\mu) \sum_{n=-\infty}^{+\infty} \frac{\cosh[\mu(n-x)]\mathrm{Im}(r_n)}{\cosh[\mu(n+1-x)]\cosh[\mu(n-1-x)]}, \tag{A2a}$$

$$\dot{x} = \frac{2\sinh(\mu)}{\mu}\sin(k) + \frac{\sinh(\mu)}{\mu} \sum_{n=-\infty}^{+\infty} \frac{(n-x)\cosh[\mu(n-x)]\mathrm{Im}(r_n)}{\cosh[\mu(n+1-x)]\cosh[\mu(n-1-x)]}, \tag{A2b}$$

$$\dot{k} = -\sinh(\mu) \sum_{n=-\infty}^{+\infty} \frac{\sinh[\mu(n-x)]\mathrm{Re}(r_n)}{\cosh[\mu(n+1-x)]\cosh[\mu(n-1-x)]}, \tag{A2c}$$

$$\dot{\alpha} = 2[\cosh(\mu)\cos(k) + \frac{k}{\mu}\sinh(\mu)\sin(k)] + \sinh(\mu) \sum_{n=-\infty}^{+\infty} \frac{(n-x)\sinh[\mu(n-x)]\mathrm{Re}(r_n)}{\cosh[\mu(n+1-x)]\cosh[\mu(n-1-x)]} - \cosh(\mu)$$
$$\times \sum_{n=-\infty}^{+\infty} \frac{\cosh[\mu(n-x)]\mathrm{Re}(r_n)}{\cosh[\mu(n+1-x)]\cosh[\mu(n-1-x)]} + k\frac{\sinh(\mu)}{\mu} \sum_{n=-\infty}^{+\infty} \frac{(n-x)\cosh[\mu(n-x)]\mathrm{Im}(r_n)}{\cosh[\mu(n+1-x)]\cosh[\mu(n-1-x)]}, \tag{A2d}$$

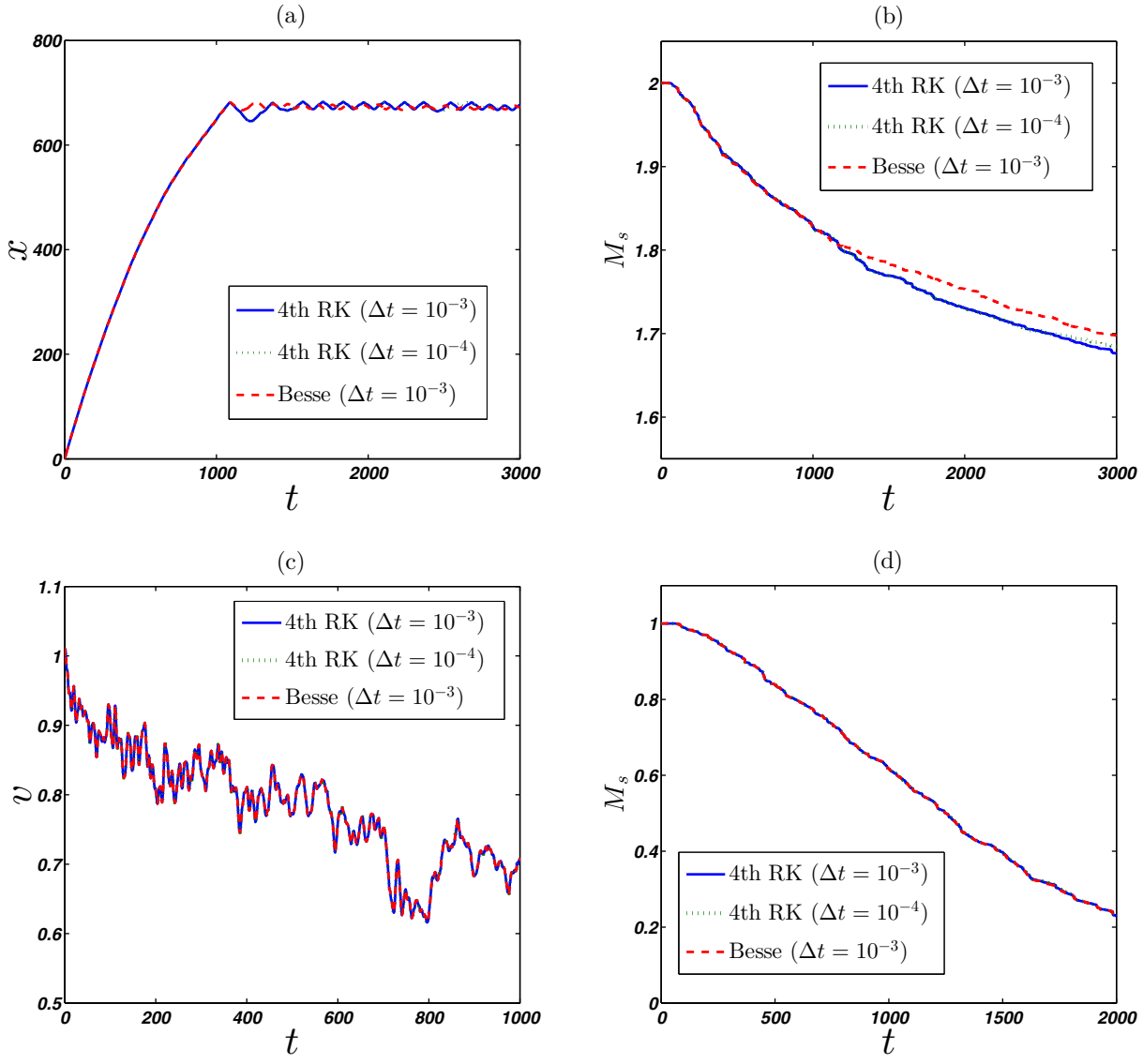

FIG. 7. (Color online) Comparison of the typical results, as for parameters of Figs. 2 and 3, integrating on Eq. (8) by the fourth-order Runge-Kutta method with different step sizes [$\Delta t = 10^{-3}$ (solid blue line) and $\Delta t = 10^{-4}$ (dotted green line)] and the Besse method with $\Delta t = 10^{-3}$ (dashed red line). (a,b) $\mu_0 = 1$, $v(t=0) = 1$, and $W = 0.1$ used in Fig. 2 with $\Delta t = 10^{-3}$; (c,d) $\mu_0 = 0.5$, $v(t=0) = 1$, and $W = 0.1$ used in Fig. 3 with $\Delta t = 10^{-3}$. The RK results of $\Delta t = 10^{-2}$ look similar.

where $r_n = R_n \exp[-ik(n-x) - i\alpha]$. For Eq. (8) with the solution form (2), we have

$$r_n = \frac{\varepsilon_n \sinh(\mu)}{\cosh[\mu(n-x)]}. \tag{A3}$$

Substituting (A3) into (A2), we obtain Eqs. (18).

APPENDIX B

In this Appendix, we will outline the derivation of Eq. (19). Taking a derivative on both sides of Eq. (5) with respect to t, one obtains

$$\frac{dP}{dt} = i \sum_{n=-\infty}^{+\infty} \left(\frac{\partial \psi_n}{\partial t} \psi_{n+1}^* + \psi_n \frac{\partial \psi_{n+1}^*}{\partial t} - \frac{\partial \psi_n^*}{\partial t} \psi_{n+1} - \psi_n^* \frac{\partial \psi_{n+1}}{\partial t} \right). \tag{B1}$$

With the help of Eq. (8), we derive the following results:

$$\frac{\partial \psi_n}{\partial t} = i[(\psi_{n-1} + \psi_{n+1})(1 + \psi_n \psi_n^*) - \varepsilon_n \psi_n], \tag{B2a}$$

$$\frac{\partial \psi_n^*}{\partial t} = -i[(\psi_{n-1}^* + \psi_{n+1}^*)(1 + \psi_n \psi_n^*) - \varepsilon_n \psi_n^*], \tag{B2b}$$

$$\frac{\partial \psi_{n+1}}{\partial t} = i[(\psi_n + \psi_{n+2})(1 + \psi_{n+1} \psi_{n+1}^*) - \varepsilon_{n+1} \psi_{n+1}], \tag{B2c}$$

$$\frac{\partial \psi_{n+1}^*}{\partial t} = -i[(\psi_n^* + \psi_{n+2}^*)(1 + \psi_{n+1} \psi_{n+1}^*) - \varepsilon_{n+1} \psi_{n+1}^*]. \tag{B2d}$$

Substituting (B2) into (B1), after simplification, we obtain

$$\frac{dP}{dt} = \sum_{n=-\infty}^{+\infty} [\varepsilon_n(\psi_n \psi_{n+1}^* + \psi_n^* \psi_{n+1}) - \varepsilon_{n+1}(\psi_n \psi_{n+1}^* + \psi_n^* \psi_{n+1})] = 2 \sum_{n=-\infty}^{+\infty} \mathrm{Re}(\psi_n \psi_{n+1}^*)(\varepsilon_n - \varepsilon_{n+1}),$$

which is Eq. (19).

APPENDIX C

In this Appendix, we will discuss the numerical accuracy of our numerical results. We used the fourth-order Runge-Kutta (RK) method to integrate Eq. (8). Although some lower-order but more efficient methods, such as the split-step Fourier method, as well as higher-order methods, including even the eighth-order RK method, have been cited in the literature [12,25], we consider the fourth-order RK to have an appropriate balance between accuracy and speed requirements. It is important to note that we use a moving coordinate system with its origin on the soliton, and we use absorbing boundary conditions, which are appropriate for the problem studied here.

To test the numerical accuracy, we have performed the following two procedures: first, we varied the step sizes for the fourth-order RK method by orders of magnitude ($\Delta t = 10^{-2}$–10^{-4}), and we found the results did not change; second, we employed a different integration scheme, a second-order relaxation scheme developed by Besse [24,25], and we found no significant changes for the soliton behaviors either. Comparison of some typical results, by the fourth-order RK method with different step sizes and by the Besse method, are presented in Fig. 7. For these reasons, the numerical results can be trusted.

[1] C. Sulem and P. L. Sulem, *The Nonlinear Schrödinger Equation: Self-Focusing and Wave Collapse* (Springer-Verlag, New York, 1999).

[2] M. J. Ablowitz and J. F. Ladik, J. Math. Phys. **16**, 598 (1975); **17**, 1011 (1976).

[3] J. C. Bronski, J. Stat. Phys. **92**, 995 (1998).

[4] E. Akkermans, S. Ghosh, and Z. H. Musslimani, J. Phys. B **41**, 045302 (2008).

[5] Y. V. Kartashov and V. A. Vysloukh, Phys. Rev. E **72**, 026606 (2005).

[6] K. Sacha, C. A. Müller, D. Delande, and J. Zakrzewski, Phys. Rev. Lett. **103**, 210402 (2009).

[7] A. B. Aceves, C. De Angelis, T. Peschel, R. Muschall, F. Lederer, S. Trillo, and S. Wabnitz, Phys. Rev. E **53**, 1172 (1996).

[8] T. Schwartz, G. Bartal, S. Fishman, and M. Segev, Nature (London) **446**, 52 (2007).

[9] A. A. Vakhnenko and Yu. B. Gaididei, Theor. Math. Phys. **68**, 873 (1986).

[10] K. Kundu, Phys. Rev. E **61**, 5839 (2000).

[11] D. Cai, A. R. Bishop, and N. Grønbech-Jensen, Phys. Rev. E **53**, 4131 (1996).

[12] P. G. Kevrekidis, *The Discrete Nonlinear Schrödinger Equation* (Springer-Verlag, Berlin, 2009).

[13] P. G. Kevrekidis, A. Khare, A. Saxena, I. Bena, and A. R. Bishop, Math. Comput. Simul. **74**, 405 (2007).

[14] S. Fishman, Y. Krivolapov, and A. Soffer, Nonlinearity **25**, R53 (2012).

[15] J. Billy, V. Josse, Z. Zuo, A. Bernard, B. Hambrecht, P. Lugan, D. Clément, L. Sanchez-Palencia, P. Bouyer, and A. Aspect, Nature (London) **453**, 891 (2008).

[16] F. G. Bass, Yu. S. Kivshar, V. V. Konotop, and Yu. A. Sinitsyn, Phys. Rep. **157**, 63 (1988).

[17] S. A. Gredeskul and Yu. S. Kivshar, Phys. Rep. **216**, 1 (1992).

[18] J. C. Bronski, J. Nonlin. Sci. **8**, 161 (1998).

[19] J. Garnier, SIAM J. Appl. Math. **58**, 1969 (1998).

[20] J. Garnier, Phys. Rev. E **63**, 026608 (2001).

[21] R. Franzosi, R. Livi, G. L. Oppo, and A. Politi, Nonlinearity **24**, R89 (2011).

[22] M. Mochol, M. Płodzień, and K. Sacha, Phys. Rev. A **85**, 023627 (2012).

[23] C. A. Müller, Appl. Phys. B **102**, 459 (2011).

[24] C. Besse, SIAM J. Numer. Anal. **42**, 934 (2004).

[25] X. Antoine, W. Bao, and C. Besse, Comput. Phys. Commun. **184**, 2621 (2013).